Supporting Information

Redon et al. 10.1073/pnas.1008260107

SI Materials and Methods

Tumor Implantation and Tissue Harvesting. The protocols for this study were approved by the National Cancer Institute Animal Care and Use Committee. One vial of a cryopreserved tumor tissue was thawed according to protocols provided by the Division of Cancer Treatment and Diagnosis repository. The tissue was minced into fragments of ≈8 mm^3 ($2 \times 2 \times 2$ mm). These tumor fragments were placed into an 11- to 13-gauge trocar. One tumor fragment of B16 melanoma or M5076 reticulum sarcoma was implanted s.c. into each of 3 B6 donor mice, and a COLON26 carcinoma was implanted into each of 3 BALB/c donor mice. A similar procedure was performed for implanting grown tumors harvested from donor mice to test cohort (TST) animals. For the purpose of restraint, all recipient mice of TST, inflammation control (IC), and negative control (NC) cohorts were anesthetized with isoflurane gas at the time of injection. Growth of tumors was monitored at least twice weekly using in situ caliper measurements to determine tumor mass. Tumor weights (Tw, in milligrams) were calculated from measurements (in millimeters) of two perpendicular dimensions (length, L; and width, W) using the approximated volume formula for a prolate ellipsoid ($V = 0.5 \times L \times W^2$) and assuming a specific gravity (Gs) of 1.0 g/cm^3 ($Tw = 0.5 \times L \times W^2 \times Gs$). Animals of the IC cohort were monitored once daily for signs of an inflammatory response at the injection site (swelling).

Mice of all three cohorts in three experiments were killed with CO_2 when grafted tumors in the test cohort reached a volume of ≈200 mg ($L = 7$ mm, $W = 5$ mm). Duodenum, colon, rectum, stomach, liver, kidney, lung, and ovary were harvested and touch-printed to a slide surface and were frozen or fixed by formaldehyde exposure and paraffin-embedded. Pathology reports were prepared for all organs of test and control mice. Necropsies following sacrifice of both donor mice and experimental mice did not show any gross nodules or masses. Metastases were not present on pathology analysis of lungs, liver, spleen, and other organs. None of the examined tissues in control and test cohorts exhibited any signs of chronic infections or physical trauma. The terminal bleeding was performed by snipping thoracic aorta and collecting blood in thoracic cavity into anticoagulant tubes (BD Biosciences) with 1 volume of PBS. Splenocytes were dispersed from spleen tissues by perfusing the RPMI medium (Invitrogen) supplemented with 10% heat inactivated FBS (Atlanta Biologicals) and 100 U/mL penicillin/100 μg/mL streptomycin (Invitrogen) on the sides of the spleen through a 25-gauge needle.

Immunohistochemistry and γ-H2AX Analysis. Touch-print specimens and frozen sections were air-dried, fixed in 2% paraformaldehyde for 20 min at room temperature, permeabilized with 1% Triton X-100, and processed for γ-H2AX immunostaining, as previously described (1). Whole-blood lymphocytes and splenocytes were separated, fixed, and prepared for γ-H2AX immunostaining as previously described (2). PBS was replaced with PBS containing 0.5% Tween-20 and 0.1% Triton X-100 (both from Bio-Rad) for blocking and antibody incubation.

γ-H2AX foci were visually counted in 100 to 500 cells in lymphocyte and splenocytes, and in several randomly examined microscopic fields (at least 300–500 cells per mouse) in tissue touch-prints and skin frozen sections. Visual counting was validated using the FociCounter software (http://focicounter.sourceforge.net/index.html) (3). Alternatively, γ-H2AX intensity in frozen sections of duodenum and skin (hair follicles) was measured using the Adobe Photoshop imaging-software package (Adobe Systems).

Paraffin sections of colon, duodenum, and skin from M5076 and COLON26 tumor-bearing and control mice, and liver and kidney from B16 tumor-bearing and control mice were subjected to the immunoperoxidase staining with inflammatory markers. These markers were biotinilated rabbit polyclonal anti-F4/80 polyclonal antibody (Invitrogen), which is a marker of maturation and activation state of tissue-infiltrating monocytes/macrophages (4), anti-CD3 (AbD Serotec), which marks mature T lymphocytes, and CD45/B220 (BD Pharmingen), which marks B-lymphocytes. Shortly, the sections were deparaffinized slides with xylene, rehydrated through 100 and 95% ethanols, incubated with the primary antibodies, biotinylated goat anti-rabbit IgG secondary antibody, and ABC Elite reagent (Vector Laboratories), and horseradish peroxidase staining was retrieved with diaminobenzidine (Sigma). Hematoxylin was used for nuclear counterstaining.

Isolation and Processing of Mouse DNA for OCDL detection. The High Pure PCR Template Kit (Roche) was used for isolation of DNA from the tissues as previously described (5, 6). To minimize oxidation artifacts during DNA isolation, all buffers were freshly prepared, autoclaved, purged with argon, and supplemented with 50 μM phenyl-tert-butyl nitrone, a free radical scavenger (Sigma-Aldrich) (7). For oxidatively induced clustered DNA lesions (OCDL) detection and measurement, an adaptation of constant-field gel electrophoresis was used along with quantitative electronic imaging, and number average length analysis (8). Human repair enzymes APE1 and OGG1 were used as damage probes along with *Escherichia coli* EndoIII (New England Biolabs) (6, 7). Detection of bistranded OCDLs was performed as described in ref. 9. Briefly, 40 ng of isolated DNA was mixed with 7 μL of the appropriate enzyme reaction buffer and left on ice for 30 min. The enzyme buffers used were: APE1 buffer (50 mM potassium acetate, 20 mM Tris acetate, 10 mM magnesium acetate, pH 7.9), OGG1 buffer (50 mM NaCl, 10 mM $MgCl_2$, 10 mM Tris-HCl, pH 7.9), and *E. coli* EndoIII buffer (20 mM Tris-HCl, 1 mM EDTA, pH 8.0).

Antioxidant Assay. The total antioxidant capacity was measured using the Antioxidant Assay Kit (Sigma-Aldrich) (10). The specific assay is based on the formation of a ferryl myoglobin radical from myoglobin and H_2O_2, which oxidizes the ABTS [2,2′-azino-bis(3-ethylbenzthiazoline-6-sulfonic acid] to produce a radical cation $ABTS^+$, which can be monitored by reading absorbance at 750 nm. In the presence of antioxidants, the radical cation is suppressed to an extent dependent on the activity of the antioxidant and the color intensity is decreased proportionally. Trolox (6-hydroxy-2,5,7,8-tetramethylchroman-2-carboxylic acid), a water-soluble vitamin E analog, serves as a standard or a control antioxidant. Approximately 100 mg of each tissue (except ovary, spleen, and rectum) were lysed by 500 μL of 1× Kit assay buffer. Whole tissue of ovary (≈15 mg), spleen (≈80 mg), and rectum (≈35 mg) were lysed by 300 μL of 1× Kit assay buffer. Tissues were homogenized by OMNI high shear homogenizer (OMNI International) on ice and centrifuged at 10,000 × g for 15 min at 4 °C. Lysates in a 96-well plate were mixed with 1× myoglobin working solution, ABTS working solution, and 3% H_2O_2, and allowed to incubate at room temperature for 5 min. Stop solution from the kit was added to each well, and the samples were read on a VersaMaxPLUS ROM plate reader (Molecular Devices). The antioxidant concentration (mM) relative to the concentration of the Trolox standard was calculated using a reference Trolox standard curve. All antioxidant concentrations were normalized by 100 mg of tissue weight.

ELISA. Eighty 100-μL mouse serum samples were obtained by terminal bleeding from B6 tumor-free or tumor-bearing mice with B16 melanoma and M5076 reticulum cell sarcoma. Blood samples were centrifuged for 5 min at maximum speed and the supernatants were collected. ELISAs were performed using the mouse inflammation and obesity ELISA strip assay from Signosis, according to the manufacturer's protocols. Tested proteins were IL-1α, IL-1β, IL-6, G-CSF, MCP-1, MIP-1a, SCF, Rantes, Leptin, TNF- α, IGF1, and VEGF. Plates were read at 450 nm on a Molecular Devices Precision Microplate Reader. In addition, the serum samples were sent to Rules-Based Medicine for independent analysis of 59 cytokines.

Statistical Analysis. The paired Student's *t* test was used to evaluate the differences between both NC and IC, and TST cohorts of mice ($P < 0.05$).

1. Rogakou EP, Boon C, Redon C, Bonner WM (1999) Megabase chromatin domains involved in DNA double-strand breaks in vivo. *J Cell Biol* 146:905–916.
2. Sedelnikova OA, et al. (2008) Delayed kinetics of DNA double-strand break processing in normal and pathological aging. *Aging Cell* 7:89–100.
3. Jucha A, et al. (2009) FociCounter: A freely available PC programme for quantitative and qualitative analysis of gamma-H2AX foci. *Mutat Res* 696:16–20.
4. Krieglstein CF, et al. (2002) Collagen-binding integrin alpha1beta1 regulates intestinal inflammation in experimental colitis. *J Clin Invest* 110:1773–1782.
5. Sutherland BM, Bennett PV, Sidorkina O, Laval J (2000) Clustered DNA damages induced in isolated DNA and in human cells by low doses of ionizing radiation. *Proc Natl Acad Sci USA* 97:103–108.
6. Gollapalle E, et al. (2007) Detection of oxidative clustered DNA lesions in X-irradiated mouse skin tissues and human MCF-7 breast cancer cells. *Radiat Res* 167:207–216.
7. Holt SM, Georgakilas AG (2007) Detection of complex DNA damage in gamma-irradiated acute lymphoblastic leukemia Pre-b NALM-6 cells. *Radiat Res* 168:527–534.
8. Sutherland BM, Georgakilas AG, Bennett PV, Laval J, Sutherland JC (2003) Quantifying clustered DNA damage induction and repair by gel electrophoresis, electronic imaging and number average length analysis. *Mutat Res* 531:93–107.
9. Nowsheen S, et al. (2008) Accumulation of oxidatively induced clustered DNA lesions in human tumor tissues. *Mutat Res* 674:131–136.
10. Francisco DC, et al. (2008) Induction and processing of complex DNA damage in human breast cancer cells MCF-7 and nonmalignant MCF-10A cells. *Free Radic Biol Med* 44:558–569.

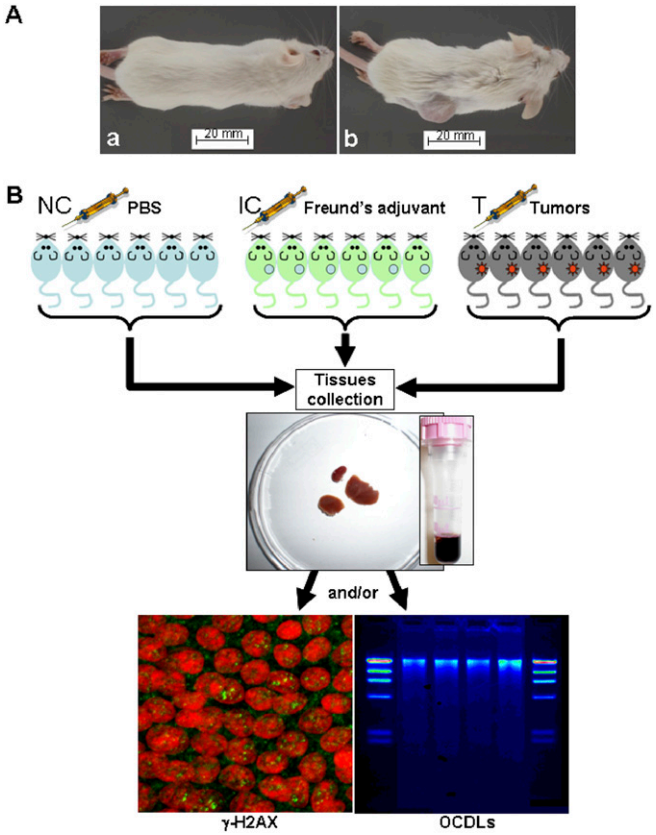

Fig. S1. Experimental scheme. (*A*) B6 or BALB/c female age-matched control mice (a) were compared with mice s.c. implanted with tumors (b). (*B*) Six-animal cohorts of mice injected with PBS (NC); mice injected with Freund's adjuvant (IC); and test tumor-bearing mice (TST), were analyzed for each experiment. When the tumors approached 200 mg, the animals were killed and various organs were examined. Samples of duodenum, colon, rectum, stomach, liver, kidney, lung, ovary, and skin, and splenic and blood lymphocytes, were taken for analysis. All samples were analyzed by immunofluorescent confocal microscopy using γ-H2AX focus formation to identify double-strand breaks. OCDLs were measured in tissue samples using human and bacterial lesion-specific repair enzymes as damage probes coupled with constant-field gel electrophoresis of the enzyme-treated DNA.

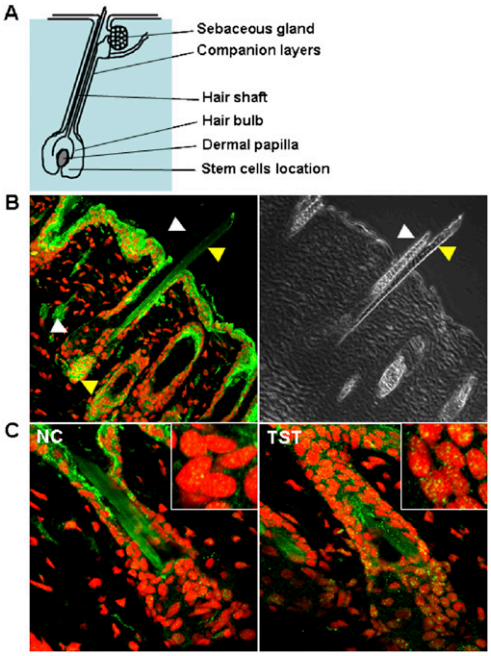

Fig. S2. γ-H2AX staining increases in hair follicles of tumor-bearing mice (data for COLON26 carcinoma experiment is presented). (*A*) Schematic drawing of a hair follicle in the growth stage. (*B*) Hair follicles at different stages of their life cycle display different intensities of γ-H2AX staining, as their sensitivity depends on many factors including growth, morphology, and proliferation activity (1, 2) (frozen skin section of a tumor-bearing mouse is presented). These changes make it challenging to quantify γ-H2AX in the hair follicles, because the signal intensity may depend on a combination of factors, likely leaving only the growth (anagen) stage suitable for analysis. γ-H2AX immunostaining (*Left*) and corresponding DIC (*Right*) images of two hairs are shown. The left hair (white arrowheads) with low γ-H2AX hair bulb staining could be, by morphological comparison with images in ref. 1 in a resting quiescent stage (telogen); the right hair (yellow arrowheads) with high γ-H2AX hair bulb staining is in an active growth stage (anagen). Notice differences in morphological structure of the two hair shafts (DIC image) and their different autofluorescent staining (immunofluorescent image). (*C*) Representative images of parallel sections of anagen hairs of NC and TST cohort mice showing increased γ-H2AX focal staining in tumor-bearing mice (magnification, 400×). Enlarged cells are shown in the *Insets*.

1. Müller-Röver S, et al. (2001) A comprehensive guide for the accurate classification of murine hair follicles in distinct hair cycle stages. *J Invest Dermatol* 117:3–15.
2. Yu BD, Mukhopadhyay A, Wong C (2008) Skin and hair: Models for exploring organ regeneration. *Hum Mol Genet* 17(R1):R54–R59.

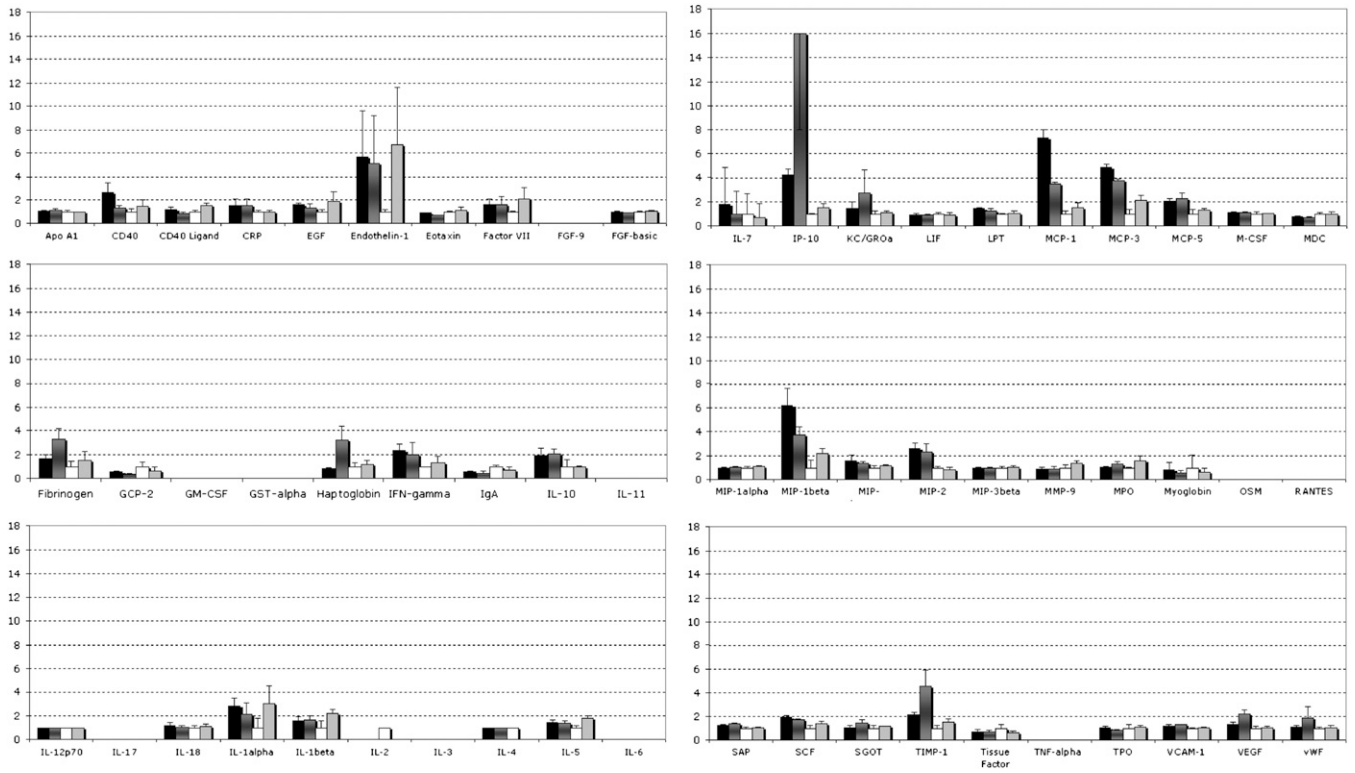

Fig. S3. Relative levels of different cytokines in serum from M5076 sarcoma-bearing mice (TST1, black bars); B16 melanoma-bearing mice (TST2, dark gray bars); NC (white bars); and IC (light gray bars) mice were analyzed by LUMINEX multiplexed immunoassays for their content in 59 factors using the RodentMAP version 2.0 antigens (Rules Based Medicine). Factor levels are shown relative to the NC control cohort. Error bars represent SDs for three mice. Blank results reflect samples not measurable because of undetectable concentrations.

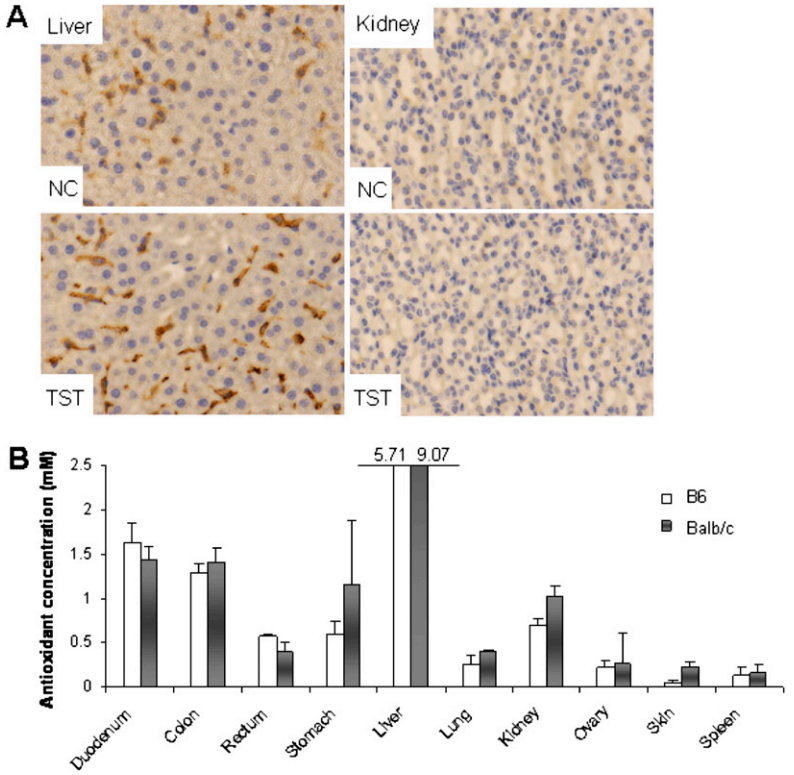

Fig. S4. (*A*) F4/80 immunoperoxidase staining of paraffin sections of liver and kidney of B16 melanoma-bearing mice (TST) compared with NC cohort. Liver contains appreciable numbers of F4/80$^+$ activated macrophages not only in TST, but also in NC animals, but kidney is completely free of F4/80 staining. Magnification: 200×. (*B*) Detection of the basal level of antioxidant capacity in intact mouse tissues. The amounts of antioxidant concentration (mM) in tissues from C57BL/6 and Balb/C relative to the concentration of the Trolox (vitamin E analog) standard were calculated using a reference Trolox standard curve. All amounts of antioxidant concentration were normalized by 100 mg of tissue weight. Liver has the highest level of antioxidant defense compared with other tissues, including skin and gastrointesinal tract tissues. Error bars are SDs (n = 3, number of mice per strain).

Table S1. Summary of the increased numbers of γ-H2AX foci and OCDL levels found in the examined tissues from three experiments

	n/a	hAPE1	ENDOIII	hOGG1
Enzyme	γ-H2AX	Abasic	OxyPy	OxyPu
B16 Melanoma				
Duodenum	2.3	1.9	2.1	2.8
Ovary	–	1.9	1.7	1.6
Lung	–	2	2.1	–
Liver	–	–	–	–
Kidney	–	–	–	–
Skin control/skin proximal	3.5	1.6	1.7	1.6
Melanoma mass	4.4	1.8	1.7	1.8
MO5076 sarcoma				
Duodenum	2.3	2.5	1.9	2.1
Colon	2.3	3	1.8	2.6
Rectum	1.7	3.3	3.2	3.3
Stomach	1.4	4.6	1.9	3.4
Skin control/skin proximal	2.3	2.5	2.9	2.8
Skin close	1.9	5	3.5	2
Sarcoma mass	3.1	2.6	4.1	2.9
COLON26 carcinoma				
Duodenum	2.8	2.2	3.8	2.8
Colon	3.7	3.1	2.7	3.6
Rectum	1.7	4.1	2.3	3.2
Stomach	1.8	1.9	1.7	1.6
Skin control/skin proximal	2.5	2	2.3	3.4
Skin close	1.5	2.3	2	3.6
Skin distal	1.6	1.8	3.1	4
Carcinoma mass	5.7	2.7	3.5	4.4

The numbers are the ratios of those values that showed significant increases comparing tissues from the TST and control cohorts. The greater of the two control values was used. "–" indicates insignificant changes.

Table S2. γ-H2AX focal values (average numbers of foci per cell) in tissues of TST, NC, and IC control cohort animals

	γ-H2AX foci per cell		
Experiment/tissue	NC (PBS)	IC (Freund's adjuvant)	TST (tumor)
B16 melanoma			
Duodenum	**1.032 ± 0.78**	**0.869 ± 1.21**	**2.303 ± 1.27***
Ovary	1.484 ± 2.06	1.126 ± 1.08	1.264 ± 1.11
Lung	0.204 ± 0.17	0.121 ± 0.15	0.243 ± 0.46
Liver	1.846 ± 1.98	2.513 ± 1.79	1.844 + 1.31
Kidney	1.432 ± 1.37	0.774 ± 0.49	0.674 ± 0.63
Skin control/ skin proximal to tumor	**0.768 + 0.05**	**0.486 + 0.05**	**2.664 ± 0.04***
Melanoma mass			**3.364 + 0.06***
Whole-blood lymphocytes	0.035 ± 0.02	0.026 ± 0.01	0.032 ± 0.01
Splenocytes	0.203 ± 0.13	0.218 ± 0.07	0.223 ± 0.13
MO5076 Sarcoma			
Duodenum	**0.346 ± 0.08**	**0.567 ± 0.28**	**1.292 ± 0.52***
Colon	**0.363 ± 0.09**	**0.366 ± 0.27**	**0.844 ± 0.13***
Rectum	**0.507 ± 0.08**	**0.426 + 0.11**	**0.875 ± 0.12***
Stomach	**0.478 ± 0.18**	**0.313 ± 0.14**	**0.652 ± 0.19***
Skin control/skin proximal to tumor	**1.300 ± 0.64**	**1.364 ± 0.47**	**3.142 ± 0.56***
Skin close			**2.551 + 0.94***
Sarcoma mass			**4.398 + 0.65***
Whole-blood lymphocytes	0.033 ± 0.005	0.032 ± 0.01	0.033 ± 0.01
Splenocytes	0.057 ± 0.02	0.091 ± 0.04	0.125 ± 0.04
COLON26 carcinoma			
Duodenum	**0.603 ± 0.33**	**0.555 ± 0.39**	**1.709 ± 0.58***
Colon	**0.266 ± 0.10**	**0.250 ± 0.11**	**0.998 ± 0.23***
Rectum	**0.593 ± 0.31**	**0.483 ± 0.14**	**1.043 + 0.21***
Stomach	**0.727 ± 0.29**	**0.636 ± 0.15**	**1.303 ± 0.46***
Skin control/skin proximal to tumor	**0.738 ± 0.38**	**0.969 ± 0.53**	**2.444 ± 0.23***
Skin close			**1.452 ± 0.43***
Skin distal			**1.515 ± 0.37***
Carcinoma mass			**5.451 + 0.31***
Whole-blood lymphocytes	0.026 + 0.01	0.025 ± 0.01	0.032 ± 0.01
Splenocytes	0.134 ± 0.10	0.165 ± 0.10	0.217 ± 0.18

The γ-H2AX focal values for the NC cohort kidney of the melanoma experiment are unexpectedly high because of high counts in three animals. Pathology reports did not reveal any kidney abnormalities or correlation with other organs' status. However, the values for the second control group, IC cohort kidney are in the range with the ones of TST cohort. The foci were visually counted in 100 to 500 cells (in lymphocyte and splenocyte cytospin preparations), and in several randomly taken microscopic fields (at least 300–500 cells per mouse) in tissue touch-prints and frozen sections. Statistically significant differences are shown in bold.

*$P < 0.05$.

Table S3. OCDL values (average numbers of abasic, oxypyrimidine, and oxypurine clusters per mega-base pair) in tissues of experimental and control animals

	hAPE1 clusters/Mbp(Abasic sites)			ENDOIII clusters/Mbp(Oxypyrimidines)			hOGG1 clusters/Mbp (Oxypurines)		
Experiment/tissue	NC (PBS)	IC (Freund's adjuvant)	TST (tumor)	NC (PBS)	IC (Freund's adjuvant)	TST (tumor)	NC (PBS)	IC (Freund's adjuvant)	TST (tumor)
B16 melanoma									
Duodenum	**0.162 ± 0.03**	**0.174 ± 0.03**	**0.326 ± 0.05***	**0.158 ± 0.03**	**0.166 ± 0.02**	**0.354 ± 0.07***	**0.108 ± 0.03**	**0.133 ± 0.02**	**0.365 ± 0.07***
Ovary	**0.098 ± 0.03**	**0.114 ± 0.02**	**0.209 ± 0.04***	**0.210 ± 0.05**	**0.244 ± 0.03**	**0.410 ± 0.07***	**0.168 ± 0.03**	**0.159 ± 0.03**	**0.270 ± 0.02***
Lung	**0.225 ± 0.04**	**0.274 ± 0.05**	**0.552 ± 0.09***	**0.184 ± 0.05**	**0.211 ± 0.05**	**0.452 ± 0.07***	0.239 ± 0.07	0.291 ± 0.06	0.334 ± 0.04
Liver	0.178 ± 0.05	0.222 ± 0.04	0.247 ± 0.07	0.220 ± 0.04	0.208 ± 0.03	0.257 + 0.05	0.319 ± 0.06	0.274 ± 0.05	0.348 ± 0.05
Kidney	0.105 ± 0.01	0.106 ± 0.01	0.138 ± 0.02	0.164 ± 0.05	0.179 ± 0.04	0.180 ± 0.03	0.280 ± 0.09	0.254 ± 0.09	0.300 ± 0.11
Skin control/skin proximal to tumor	**0.193 ± 0.02**	**0.196 ± 0.02**	**0.320 ± 0.04***	**0.216 ± 0.02**	**0.183 ± 0.04**	**0.360 ± 0.06***	**0.333 ± 0.04**	**0.306 ± 0.04**	**0.539 ± 0.08***
Melanoma mass			**0.345 ± 0.03***			**0.378 ± 0.04***			**0.587 ± 0.006***
MO5076 sarcoma									
Duodenum	**0.131 ± 0.02**	**0.137 ± 0.01**	**0.318 ± 0.06***	**0.149 ± 0.02**	**0.156 ± 0.02**	**0.307 ± 0.06***	**0.199 ± 0.03**	**0.235 ± 0.03**	**0.479 ± 0.10***
Colon	**0.201 ± 0.04**	**0.232 ± 0.04**	**0.685 ± 0.13***	**0.185 ± 0.02**	**0.241 ± 0.04**	**0.438 ± 0.06***	**0.257 ± 0.04**	**0.261 ± 0.05**	**0.668 ± 0.11***
Rectum	**0.123 ± 0.02**	**0.196 ± 0.07**	**0.659 ± 0.14***	**0.149 ± 0.04**	**0.061 ± 0.01**	**0.483 ± 0.05***	**0.093 ± 0.02**	**0.145 ± 0.06**	**0.501 ± 0.08***
Stomach	**0.144 ± 0.02**	**0.172 ± 0.01**	**0.775 ± 0.08***	**0.146 ± 0.01**	**0.164 ± 0.01**	**0.294 ± 0.04***	**0.155 ± 0.02**	**0.179 ± 0.02**	**0.609 ± 0.11***
Skin control/skin proximal to tumor	**0.242 ± 0.02**	**0.222 ± 0.03**	**0.598 ± 0.08***	**0.166 ± 0.02**	**0.133 ± 0.02**	**0.523 ± 0.09***	**0.231 ± 0.05**	**0.192 ± 0.03**	**0.646 ± 0.04***
Skin close			**0.393 ± 0.06***			**0.592 ± 0.08***			**0.466 ± 0.05***
Sarcoma mass			**0.631 ± 0.04***			**0.685 ± 0.12***			**0.661 ± 0.08***
COLON26 carcinoma									
Duodenum	**0.230 ± 0.04**	**0.250 ± 0.03**	**0.563 ± 0.06***	**0.172 ± 0.02**	**0.153 ± 0.02**	**0.646 ± 0.05***	**0.239 ± 0.04**	**0.191 ± 0.02**	**0.675 ± 0.04***
Colon	**0.140 ± 0.02**	**0.166 ± 0.01**	**0.528 ± 0.04***	**0.181 ± 0.01**	**0.193 ± 0.03**	**0.509 ± 0.03***	**0.137 ± 0.01**	**0.158 ± 0.02**	**0.571 ± 0.05***
Rectum	**0.204 ± 0.03**	**0.279 ± 0.03**	**0.687 ± 0.05***	**0.171 ± 0.02**	**0.223 + 0.02**	**0.505 ± 0.04**	**0.144 ± 0.01**	**0.192 ± 0.03**	**0.591 ± 0.06***
Stomach	**0.215 ± 0.03**	**0.216 ± 0.05**	**0.416 ± 0.07***	**0.201 ± 0.04**	**0.176 ± 0.03**	**0.328 ± 0.04***	**0.315 ± 0.03**	**0.249 ± 0.04**	**0.517 ± 0.06***
Skin control/skin proximal to tumor	**0.232 ± 0.02**	**0.176 ± 0.02**	**0.462 + 0.06***	**0.221 ± 0.04**	**0.139 ± 0.04**	**0.505 ± 0.08***	**0.214 ± 0.02**	**0.197 + 0.03**	**0.714 ± 0.09***
Skin close			**0.531 ± 0.07***			**0.442 ± 0.10***			**0.755 ± 0.06***
Skin distal			**0.420 ± 0.05***			**0.682 ± 0.09***			**0.848 ± 0.07***
Carcinoma mass			**0.631 ± 0.04***			**0.778 ± 0.11***			**0.931 ± 0.09***

OCDLs were measured in tissue samples isolated DNA using appropriate human or bacterial lesion-specific repair enzymes as damage probes coupled with a constant-field gel electrophoresis. Statistically significant differences are shown in bold.

*$P < 0.05$.